AIG Journal

Published by the Australian Institute of Geoscientists

ISSN 1443-1017

Wavelet Tessellation and its Application to Downhole Gamma Data from the Manyingee & Bigrlyi Sandstone-Hosted Uranium Deposits

A. Wilde[1], E.J. Hill[2], S. Schmid[2] & W.R. Taylor[3]

[1] Centre for Exploration Targeting, University of Western Australia, Crawley, Western Australia
[2] CSIRO, Mineral Resources, Kensington, Western Australia
[3] Energy Metals Ltd, West Perth, Western Australia

Abstract

Measurement of natural gamma radiation in drillholes can be important for lithology identification, correlation of sedimentary layers between drillholes, in studies of hydrothermal alteration and in geometallurgy *inter alia*. Traditional interpretation of gamma data for these purposes has typically been by subjective visual analysis. In this paper we discuss the application of a new technique: wavelet tessellation (Hill et al. 2015). Tessellation automatically picks boundaries in depth-attributed numeric data and attributes the area between the boundaries with an average of the data, in this case gamma radiation in counts per second. We show that tessellation of gamma data is a valuable adjunct to traditional visual lithological logging using examples from the Manyingee and Bigrlyi uranium deposits. Tessellation can rapidly and reproducibly resolve important detail in the rocks that is not detectable by the human eye and should be considered an important addition to the toolkit of the mining and exploration geoscientist.

Introduction

Lithological logging of drillholes is beset with uncertainty, particularly when only small and relatively fine-grained rock chip samples are recovered. It can be difficult to recognise lithology with confidence and to establish subtle variations in apparently homogeneous sequences of sandstone or mudstones that may be important for correlation or be indicative of ore-related hydrothermal alteration. Measurement of natural gamma radiation can help in this regard, indeed, wireline gamma tools have been used in lithological logging since 1936 (Hilchie, 1990). Traditional interpretation of gamma data for these purposes has typically been by subjective visual analysis.

Subjective visual analysis of gamma data can be effective, but it is time-consuming and results may differ substantially between different interpreters. The wavelet transform has been used as an objective boundary detection method for wireline logging (Cooper and Cowan, 2009; Arabjamaloei et al., 2011; Perez-Munoz et al., 2013; Davis and Christensen, 2013). The results of the wavelet transform are typically displayed as a scale-space plot (also known as a scaleogram), but are difficult to interpret except by an expert in wavelet methods (Figure 1a). Hill et al. (2015) proposed the use of the wavelet tessellation as an improved visualisation of the scale-space plot. The tessellation is intuitive to geologists as it resembles a traditional geology log but with multiple scales of boundary selection (Figure 2). In this contribution we demonstrate the use of the wavelet tessellation method and illustrate its ability to detect obscure boundaries and to precisely locate boundaries in monotonous sedimentary sequences from the sandstone-hosted uranium deposits of Manyingee (Western Australia) and Bigrlyi (Northern Territory, Australia; Figure 3.)

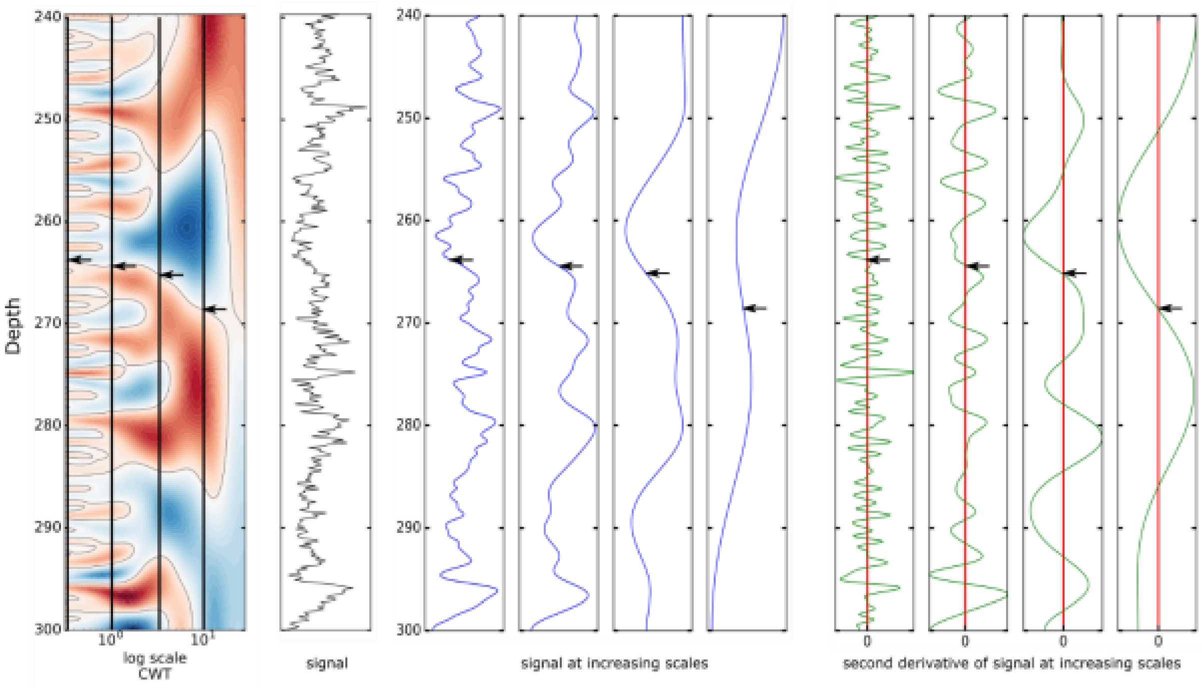

. (a) (b) (c) (d)

Figure 1: The effect of increasing scale on the wavelet transform of the signal is illustrated by showing the shape of the signal at 4 selected scales (i.e. 0.3, 1.0, 3.3, 10) depth is in metres. (a) Scale-space plot of continuous wavelet transform, grey lines are zero contours, vertical black lines indicate the 4 illustrated scales ; (b) gamma signal as log counts; (c) progressive smoothing of the gamma signal with increasing scale, arrows indicate inflection points on one boundary; (d) progressive smoothing of the 2nd derivative of the gamma signal; arrows indicate zero crossing points on one boundary.

Wavelet Tesselation Applied to Gamma Data

Downhole Gamma Logs

Much of the natural gamma radiation emanating from rocks is due to the presence of radioactive K^{40}, U^{238} and Th^{232} (Firth, 1999). Downhole gamma logs are highly sensitive indicators of the variation in these elements and in many cases permit effective discrimination between different rock types or of subtle variation (such as bedding or degree of hydrothermal alteration) within individual rock types.

A formula to estimate the relative contributions of the three radioactive elements to total gamma response is (Crain, 2016):

$$\text{Gamma}_{\text{tot}} = (\text{K\%} * 16) + (\text{U ppm} * 8) + (\text{Th ppm} * 4)$$

In unmetamorphosed sedimentary rocks, the low abundance of U and Th means that the gamma response is controlled mainly by potassic phyllosilicates such as muscovite or by potassium feldspar. In U-mineralised rocks, however, the gamma response due to U generally overwhelms that due to K or Th.

Wavelet Tessellation Method

The wavelet tessellation method of Hill et al. (2015) was developed in order to determine the downhole location of lithological contacts from geochemical data but is applicable to any continuous numerical data, including natural gamma logs. The technique allows signal boundaries to be detected over a range of scales and uses the 2nd order derivative of Gaussian wavelet (DOG) because it has special properties which allow the transform to be converted to a tessellation (Fig. 2; Witkin, 1983).

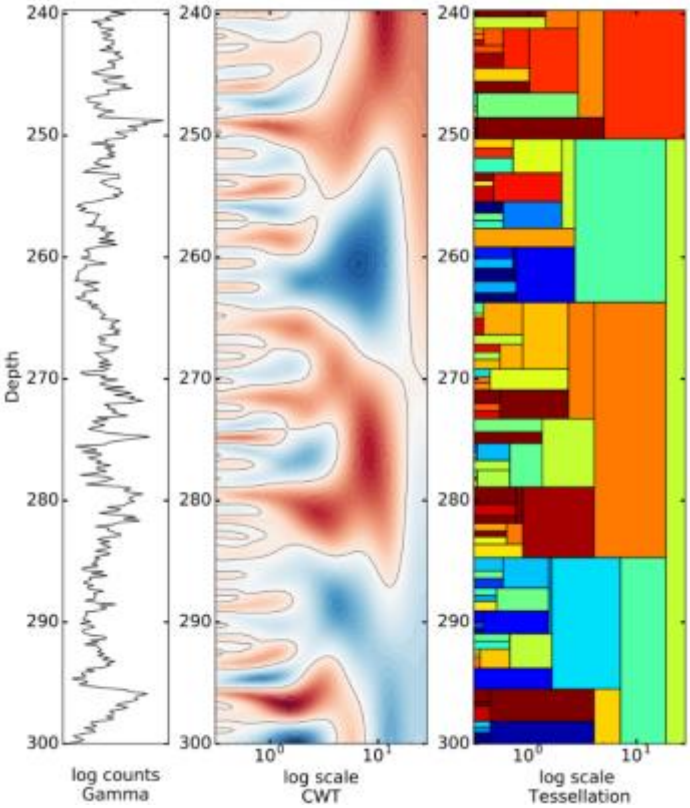

. (a) (b) (c)

Figure 2: (a) Log gamma counts for subsection of drill hole 240-300 m. (b) Scale-space plot of continuous wavelet transform. (c) Tessellation of scale-space plot (GWT plot). Colours indicate mean values of each interval represented by a rectangle; cool colours = low values, warm colours= high values. Boundaries in the tessellation are depth corrected using the location of zero contours at the smallest scale. Rectangles on the left side of the plot represent small scale spatial domains and domains of increasingly larger scales to the right.

The important properties are that the zero contours at any scale can be traced to the smallest scale and that the depth at the smallest scale is the best estimate of the depth of the boundary. The DOG wavelet has been extensively studied for its favourable properties for edge detection in images and for image compression (for example, Mallat, 1991; Mallat and Hwang, 1992; Mallat and Zhong, 1992). The zero crossings of the 2nd derivative of a signal represent the inflection points in the signal (Fig. 1c), which also represent an intuitive estimate of the location of boundaries. The increasing scales in the wavelet transform result from increasing the width of the wavelet, this has the effect of progressively smoothing the signal as the scale increases resulting in smoothing out of the smaller scale features (Fig. 1c). For a comprehensive mathematical description of the continuous wavelet transform method the reader is referred to Mallat (2009). The continuous wavelet transform used in this paper is based on the algorithm of Torrence and Compo (1998) and the tessellation method is based on the description in Witkin (1983). The full gamma wavelet tessellation (GWT) method is described in Hill et al. (2015). Algorithms were coded using the Python programming language.

Geological Background

Manyingee

The Manyingee and Manyingee East roll front uranium deposits are located 85 km SSE of Onslow, in Western Australia (Figure 3). Drillholes have penetrated a sequence of flat-lying Cretaceous and younger lithologies of the Carnarvon Basin (Valsardieu et al., 1981; Wilde et al., 2013; Wilde et al., in press). The Cretaceous rocks occupy well-defined palaeochannels and rest directly on Proterozoic granitic basement rocks at depths of up to 150 m below the surface. Basal conglomerate (Yarraloola Conglomerate) overlies disaggregated granitic basement rocks (logged as arkose but probably grus) and is succeeded by the principal host unit to uranium, the alluvial and fluvial Birdrong Sandstone (Valsardieu et al., 1981). The Birdrong Sandstone consists of thin conglomeratic sandstone, sandstone and rare carbonaceous mudstone. The sequence is overlain by the Cretaceous Muderong Shale, Mardie Greensand Member and younger sediments related to contemporary drainages including clays, silts and gravel.

Figure 3. Location of sandstone-hosted uranium deposits: Manyingee, Western Australia and Bigrlyi, Northern Territory, Australia.

The mineralogical composition of the Birdrong Sandstone is summarised in Table 1. The sandstones typically contain 75% clasts and 25% matrix in addition to pores. Porosity makes up about a third of the rock volume (Table 2). Over 90% of the clasts are quartz and lithic fragments (as determined by optical microscopy). The other 10% are K-feldspar and mica, mainly biotite. Matrix minerals include siderite, goethite, kaolinite and smectite. Thus the bulk potassium content of the rock is likely to be controlled by the abundance of detrital minerals and lithic fragments, while the matrix is essentially potassium-free. The bulk potassium content is quite low, averaging 0.6% (Table 3).

The U and Th content of the sandstone is likely to be controlled by the detrital heavy mineral suite, abundance of organic matter (onto which uranium has been absorbed) and by uranium phases introduced during the formation of roll-front type mineralisation (Valsardieu et al., 1981; Wilde et al., 2013). For relatively U-poor (<50 ppm U) sandstones in sampled drillholes the average U and Th contents are 25 and 9 ppm respectively (Table 3). Heavy minerals in the Manyingee sandstones include tourmaline, zircon, garnet, kyanite and epidote, but their U and Th contents are not known.

Claystone (logged as shale) at Manyingee often has a higher gamma response in downhole logs. No mineralogical data are available for this claystone but we surmise that the gamma response is a function of higher volumes of potassic clays.

Five drillholes from the Manyingee East deposit were selected to determine the utility of the GWT method at this deposit. These holes were drilled using the mud rotary technique with lithological samples obtained at 1m intervals. Downhole gamma logs were obtained using a conventional wireline gamma tool sampling every 5 cm.

			CLASTS					MATRIX MINERALS			
Redox State	**Lithology**	**# Samples**	**Quartz**	**Lithic Fragments**	**K-Feldspar**	**Mica**	**Clast %**	**Opaques**	**Siderite**	**Clay**	**Matrix %**
REDUCED	Sandstone	2	61	22	0	2	87	2	5	6	13
	Clayey Sandstone	5	50	12	6	4	71	3	3	23	29
	Sideritic Sandstone	11	56	7	3	3	68	2	19	11	32
	AVERAGE		**56**	**14**	**3**	**3**	**75**	**2**	**9**	**13**	**25**
OXIDISED	Clayey Sandstone	2	50	20	7	3	71	6	3	23	29
	Sideritic Sandstone	2	73	0	3	1	77	5	8	10	23
	Goethitic Sandstone	7	44	11	3	5	59	20	0	24	41
	Goethitic Conglomerate	4	29	43	3	2	80	11	0	8	20
	AVERAGE		**49**	**19**	**4**	**3**	**72**	**11**	**3**	**16**	**28**

Table 1. Modal mineralogy of Birdrong Sandstone samples from Manyingee (F. Radke, unpub. data).

Sandstone Grain-Size	**Number of Samples**	**Porosity %**	**Permeability (mD)**	
			Average	**Min – Max**
Fine-Medium	2	28.9	144	1 – 287
Medium	9	32.8	1466	1 – 4042
Medium-Coarse	3	34.7	2376	1383 – 3904
Conglomeratic	5	23.1	109	0.1 - 328

Table 2: Range in sandstone porosity and permeability with respect to grain size (Anonymous, 1981).

		K (%)			**U (ppm)**			**Th (ppm)**			**Contribution to Total**		
		Mean	Max	Min	Mean	Max	Min	Mean	Max	Min	K	U	Th
MANYINGEE	Sandstone (<50 ppm U)	0.54	3.22	0.15	25	50	2	9.4	50	2	3.0	70	26
	All sandstone	0.59	3.88	0.09	341	7400	2	10	55	2	0.3	97	3
BIGRYLI	Sandstone (<50 ppm U)	2.85	3.93	1.75	6.7	35.5	1.7	11.6	34.4	5.3	23.8	28	48
	All sandstone	2.79	3.93	1.75	589	14074	1.7	12.5	42.9	5.3	0.9	97	2

Table 3: Summary of radioactive element concentrations at Manyingee & Bigrlyi.

Bigrlyi

The Bigrlyi uranium and vanadium deposit is hosted within the Carboniferous Mount Eclipse Sandstone, Ngalia Basin. In contrast to the Carnarvon Basin, the Ngalia Basin is deformed and bedding at Bigrlyi dips steeply (Schmid and Quigley, 2014). The Mount Eclipse Sandstone was deposited as stacked fluvial channel deposits intercalated with floodplain (playa) facies deposited under arid conditions (Schmid and Quigley, 2014).

The Mt Eclipse Sandstone at Bigrlyi shows little visual variation, and typically consists of medium- to coarse-grained sub-arkosic sandstones. Uranium typically occurs at the boundary between “oxidised” hematite-bearing sandstones and “reduced” kaolinised sandstone (Schmid et al., 2011).

An average sandstone sample contains approximately 65% quartz, 10% K-feldspar and 5% mica (mainly detrital biotite and muscovite) and various volumes of matrix-filling hematite, kaolinite, corrensite (interlayered smectite/chlorite), calcite and dolomite. Indicative analytical data presented in Table 3 and Figure 4 suggest that the gamma response of Bigrlyi sandstones is likely to be due to a combination of all three radioactive elements. The bulk potassium content of unmineralised sandstone (< 50 ppm U) is controlled largely by the abundance of detrital K-feldspar and mica. Uraninite and coffinite abundance controls the uranium abundance in mineralised samples.

Four diamond drillholes were selected from the Bigrlyi deposit in order to assess the value of performing GWT on the gamma data: B06016, B07074, B07120 and B09049.

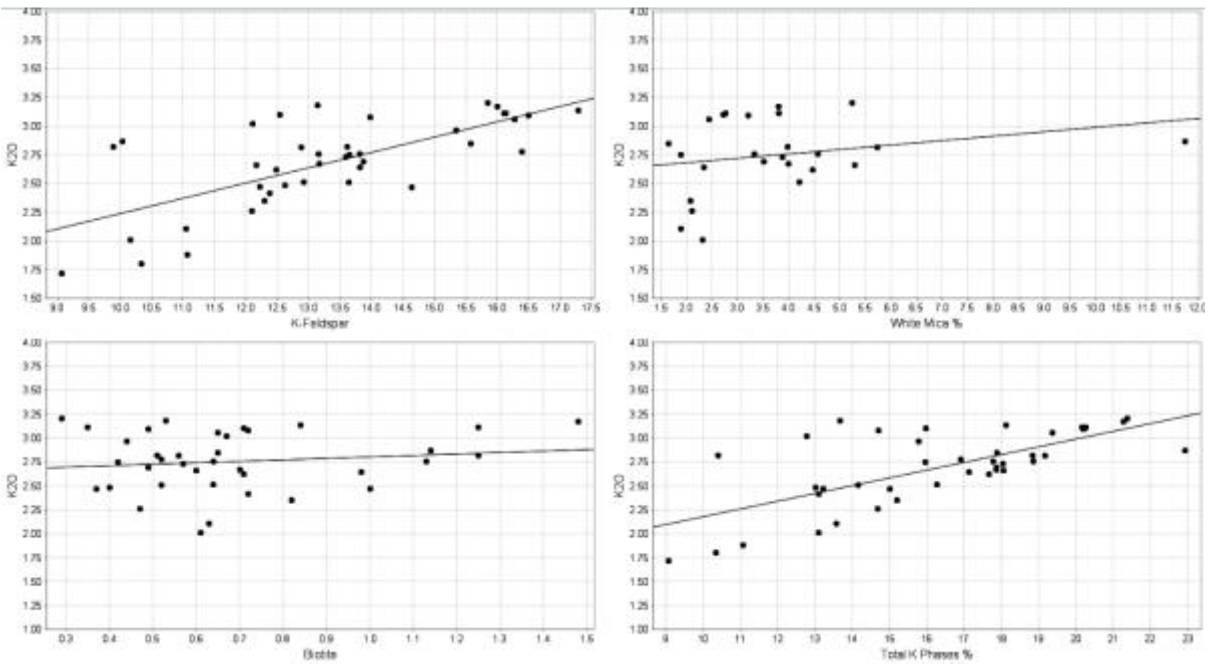

Figure 4. Relationship between Mount Eclipse Sandstone K2O content and abundance of K-bearing phases (data of Schmid and Quigley, 2014).

Results

Manyingee

Figure 5 shows the GWT for one of the Manyingee holes, MRM017. The main boundaries inferred from the GWT are shown as red lines. The correspondence between these boundaries and those picked by the logging geologists may vary by several metres.

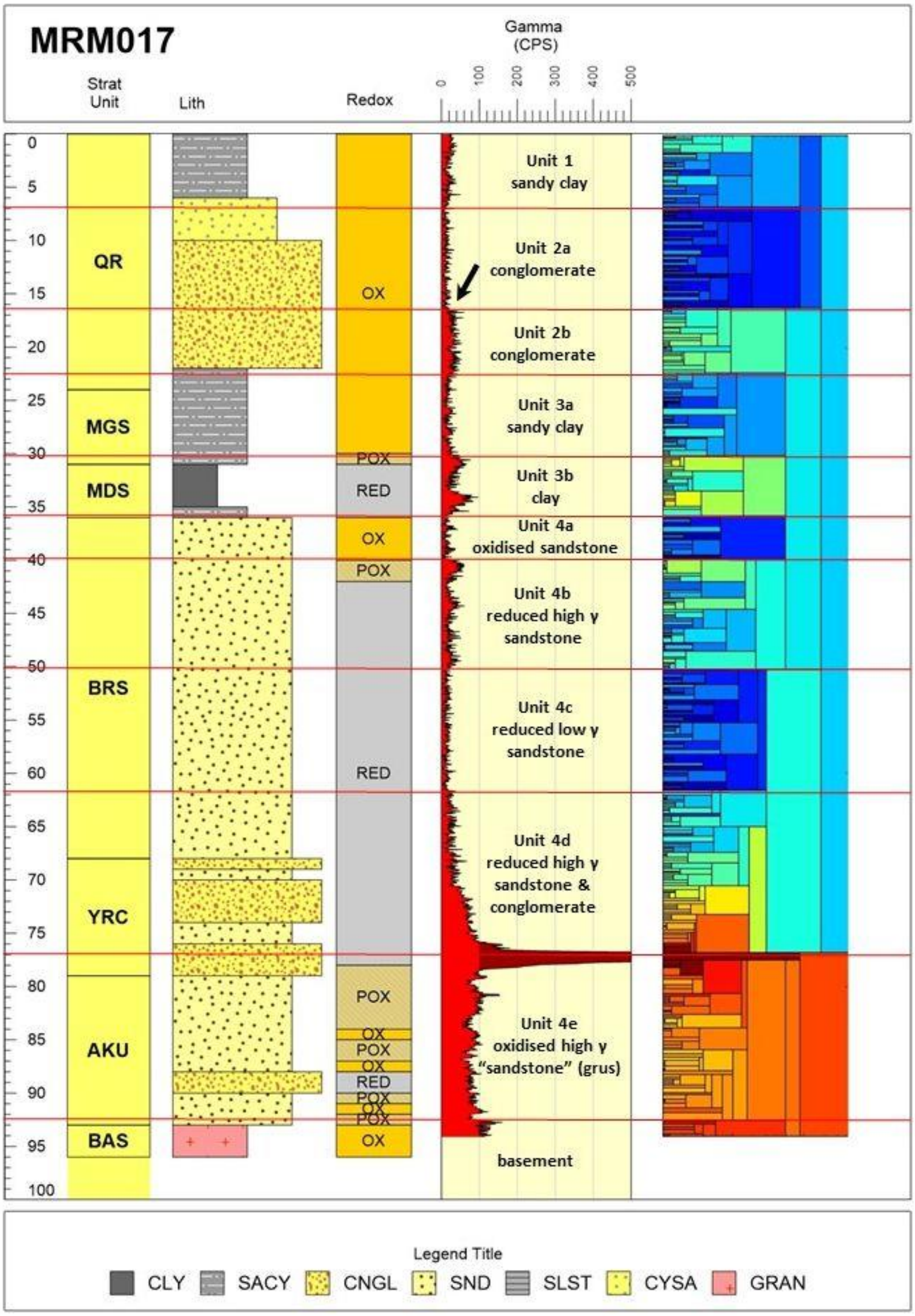

Figure 5. An example GWT from Manyingee drillhole MRM017. The first column represents the stratigraphic unit based on visual logging of chip samples collected at 1m intervals downhole. QR - Quaternary cover, MGS - Mardie Greensand Member; MDS - Muderong Shale; BRS - Birdrong Sandstone; YRC - Yarraloola Congolmerate; AKU - Basal 'arkose'; BAS - Basement granite. The second column represents the most abundant lithology unit based on visual logging of chip samples. The third column represents the inferred redox state of the chip samples: RED – reduced, POX – partially oxidised, OX – oxidised and UN – unknown. Major rock unit boundaries as inferred from the wavelet tessellation are indicated by horizontal red lines.

This discrepancy can be readily explained by the relatively imprecise depth discrimination of the rotary mud drilling technique. Downhole gamma logging is much more precise and accurate, probably to within centimetres.

The GWT reveals much lithological detail that is not resolved by the visual logging. For example the conglomerate unit in the upper part of the hole is resolved into discrete high and low gamma beds with a boundary at approximately 16m depth (arrowed). Considerable detail is also revealed within the two conglomerate units by the GWT, with many boundaries at a scale of metres or less. As the rotary mud samples represent an aggregation of at least a one metre long interval of rock, it is not possible to precisely determine what lithological variations are responsible for the variation in gamma response.

The GWT suggests that the top of the clay assigned to the Muderong Shale (MDS) is at a depth of 30m, 1m higher than logged visually, and that it can be sub-divided into three distinctive layers. The top of the crucial Birdrong Sandstone host unit as picked from the GWT agrees well with that from the visual log, which corresponds to the depth of the first recovery of sand-sized particles. The GWT, however, defines several distinct layers within the Birdrong Sandstone that are not differentiated in visual logging (units 4a-c; Figure 5). A substantial boundary is indicated at 61.5m which may be the top of the Yarraloola Conglomerate rather than 68m interpreted without the aid of gamma data. Alternatively this boundary may represent the top of a fining upwards sequence within the Birdrong Sandstone. The major boundary at 77m is no doubt influenced by the presence of uranium mineralisation, but also separates high and low gamma "domains" and is 2m higher than the contact between the Yarraloola Conglomerate and "arkose" (or grus) inferred from visual logging.

This example shows the considerable potential of the GWT to aid in stratigraphic and lithological interpretation of downhole samples. Even more detail is available in the GWT but to ascertain its significance would require correlation with a continuous sample medium such as core. These conclusions are likely to apply to other deposit types and commodities.

Bigrlyi

Drillhole (B06016) has been visually logged by several different geologists and thus GWT can afford a means of assessing disparate lithological interpretations. There is generally poor correspondence between boundaries determined by conventional visual logging and from the GWT. We note, however, that the correspondence between different visual logs is also poor (Figure 6). One possibility is that the depths recorded on the drillcore are inaccurate. However, comparison of the gamma log with radiometric measurements taken directly on the core suggests that depth mismatch is not an issue for hole B06016. It is clear, therefore, that the gamma tessellation is responding to subtle fluctuations in sandstone mineralogy namely the presence of distinct cyclical variations within the visually bland and homogeneous sandstone (Figure 6).

Discussion and Conclusions

Measurement of natural gamma radiation in drillholes can be important for lithological identification, correlation of sedimentary layers between drillholes, in studies of hydrothermal alteration and in geometallurgy *inter alia*. Downhole gamma logging for these purposes has been carried out for many decades, particularly in hydrocarbon and coal exploration. Traditional interpretation of gamma data has typically been by subjective visual analysis, although automated interpretation has been undertaken in the hydrocarbon industry (Gill, 1970). Gamma logging is undertaken relatively uncommonly in metals exploration and mining and automated processing of downhole gamma data is also uncommon.

In this paper we have illustrated the use of the wavelet tessellation technique which automatically picks boundaries in depth-attributed numeric data and attributes the area between the boundaries with an average of the data. In this case, the data used were total count gamma radiation in counts per second, which is a function of K, U and Th content of the rocks being measured. We have shown that tessellation of gamma data can be a valuable adjunct to traditional visual lithological logging using examples from the Manyingee and Bigrlyi uranium deposits.

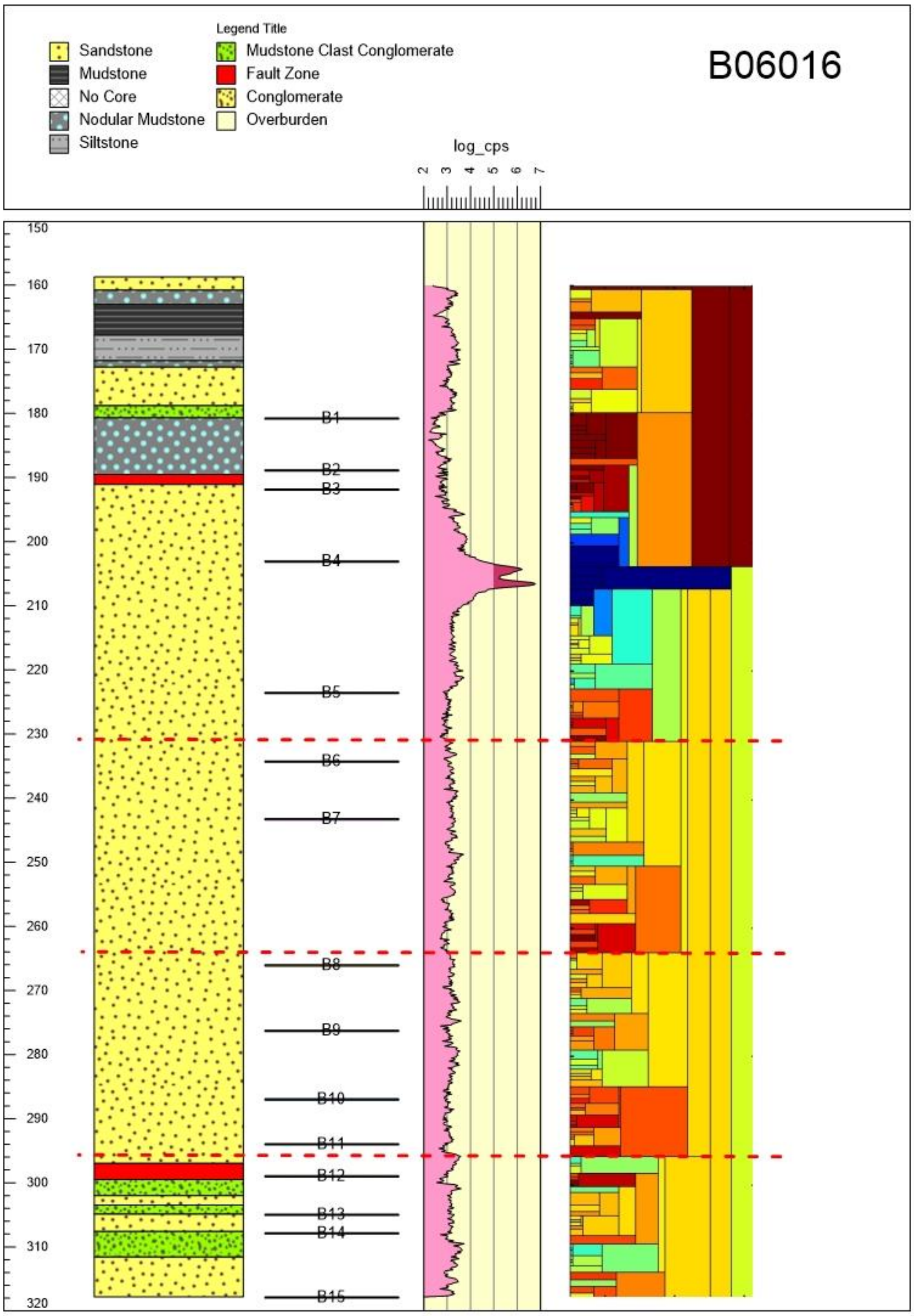

Figure 6. An example GWT from Bigrlyi drillhole B06016. Visual lithological logs from two sources are presented. Log 2 shows only major interpreted sequence boundaries. Major rock unit boundaries (fining upward sequences) as inferred from the wavelet tessellation are indicated by horizontal red lines. Note that the GWT analysis reveals subtle cyclical variation between 200 & 300m within otherwise visually monotonous sandstone

Tessellation can rapidly and reproducibly resolve subtle or subjective detail in the rocks that is not detectable by the human eye. For example, the cyclic pattern of low versus high gamma response and their upward variation can be interpreted as a function of quartz versus K-feldspar/K-phyllosilicates content. The mineralogical variations in fluvial sandstones is often a function of grain size. Therefore, the gamma tessellation may capture cyclicity related to subtle grain size variations. In Manyingee, the data can be interpreted as four fining upward sequences above the mineralisation, but an overall coarsening upward across the four cycles, which corresponds to lithological observations. At Bigrlyi, there are three fining upward cycles within the thick homogeneous sandstone (190-295m) hosting the mineralisation towards the upper contact. Thus, both examples show a pattern of cyclicity, which is impossible to identify visually, but important to understand the depositional environment and sedimentary architecture.

The technique should therefore be considered an important addition to the toolkit of the mining and exploration geoscientist. This is particularly true where the only lithological data are derived from 1m composite intervals of rock chips, such as in the rotary mud drilling method. Furthermore, routine use of GWT will help to better define the depth of rock boundaries.

The underlying reasons for the variation in gamma response in the rocks, however, may not always be obvious as is the case for the Bigryli drillhole B06016. In this case further research may be required to establish the nature of the cyclicity identified by GWT. For example, use of a portable XRF could establish the absolute abundances of K, U and Th and hence whether heavy minerals (U, Th) or feldspar or clays (K) dominate the gamma responses.

References

Anonymous, 1981, Core Analysis Results. *Core Labs. Inc. Report WA-CA-118*, 5pp.

Arabjamaloei, R.; Edalatkha, S.; Jamshidi, E.; Nabaei, M.; Beidokhti, M. and Azad, M., 2011**.** Exact lithologic boundary detection based on wavelet transform analysis and real-time investigation of facies discontinuities using drilling data. *Petroleum Science and Technology, 29*, pp. 569-578

Cooper, G. and Cowan, D., 2009**.** Blocking geophysical borehole log data using the continuous wavelet transform. *Exploration Geophysics, 40*, pp. 233-236

Crain E.R., 2016, Crain's Petrophysical Handbook: *https://www.spec2000.net/07-grlog.htm*

Davis, A. and Christensen, N., 2013**.** Derivative analysis for layer selection of geophysical borehole logs *Computers and Geosciences, 60*, pp. 34-40

Firth D., 1999, Log Analysis for Mining Applications. *Reeves Wireline Services, 159 pp*.

Gill D., 1970, Application of a Statistical Zonation Method to Reservoir Evaluation and Digitized-Log Analysis. *AAPG Bulletin, V54/5,* pp. 719-729.

Gunn, D.E., and Best, A.I., 1998, A new automated non-destructive system for high resolution multi-sensor core logging of open sediment cores. *Geo-Marine Letters, 18,* pp. 70-77.

Hilchie, D. W., 1990, Wireline: A history of the well logging and perforating business in the oil fields. Boulder, Colorado: Privately Published, 200 pp.

Hill E.J., Robertson J., & Uvarova Y., 2015, Multiscale hierarchical domaining and compression of drill hole data. *Computers & Geosciences V79,* pp. 47-57*.*

Mallat, S., 1991. Zero-crossings of a wavelet transform. *IEEE Transactions on Information Theory V37,* pp. 1019-1033.

Mallat, S. and Hwang, W. L., 1992. Singularity detection and processing with wavelets. *IEEE Transactions on Information Theory, V38,* pp. 617-643*.*

Mallat, S. and Zhong, S., 1992. Characterisation of signals from multi-scale edges. *IEEE Transactions on Pattern Analysis and Machine Intelligence V14,* pp. 710-732.

Mallat, S., 2009. A Wavelet Tour of Signal Processing 3rd Edition, Elsevier. Chapter 6, pp. 205-261.

Perez-Munoz, T.; Velasco-Hernandez, J. and Hernandez-Martinez, E., 2013**.** Wavelet transform analysis for lithological characteristics identification in siliciclastic oil fields. *Journal of Applied Geophysics, 98*, pp. 298-308

Schmid S., Foss C., Hill J., Quigley M., Schaubs P., Cleverley J. and Robinson J., 2011, Report on the JSU Ngalia Basin Uranium Mineral System Project: 102 pp.

Schmid S., & M. A. Quigley, 2014, Fluvial architecture and diagenesis of the Mt Eclipse Sandstone, northern Ngalia Basin, Australia: *Australian Journal of Earth Sciences: An International Geoscience Journal of the Geological Society of Australia*, *V61/8,* pp.1081-1094.

Torrence, C. & Compo, G. P., 1998. A practical guide to wavelet analysis. *Bulletin of the American Meteorological Society, 79*, pp. 61-78.

Valsardieu C.A., Harrop D.W. and Morabito J., 1981. Discovery of Uranium Mineralization in the Manyingee Channel Onslow Region of Western Australia. *Proc. Australian. Inst. Min. Metall. 279,* pp. 4-7.

Wilde A., Sugden S. and Thom J., 2013. Bulk Chemistry, Infra-red Spectroscopy and Geometallurgy of Paladin's Manyingee Deposit, Carnarvon Basin, Western Australia. *AIG Conference on Advances in Exploration and Ore Deposit Geochemistry, Como, Western Australia,* pp. 16-17.

Wilde A., Corbin J-C. and Thom J., in press. Manyingee Uranium Deposit. *Ore Deposits of Australia, Australasian Institute of Mining and Metallurgy, Melbourne.*

Witkin, A. P., 1983. Scale-space filtering. *Proceedings 8th International Joint Conferences on Artificial Intelligence, Karlsruhe, Germany,* pp. 1019-1022.

ACKNOWLEDGEMENTS

The work has been supported by the Deep Exploration Technologies Cooperative Research Centre (DET CRC) whose activities are funded by the Australian Government's Cooperative Research Centre Programme. This paper is DET CRC document number 2016/939. Energy Metals Ltd. and CSIRO are also thanked for permission to publish this manuscript.

AIG Journal Paper N2017-001
Received 15 Dec 2016
Reviewed 21 Jun 2017
Accepted 22 Jun 2017
Published 25 Jun 2017